Characterization of the hyperfine interaction in europium-doped yttrium orthosilicate and europium chloride hexahydrate

J. J. Longdell,* A. L. Alexander, and M. J. Sellars

Laser Physics Center, Research School of Physical Sciences and Engineering, Australian National University, Canberra, Australia

We present characterization of the hyperfine interaction for the europium in hydrated europium chloride and as a dopant in yttrium orthosilicate. The Zeeman and pseudoquadrupole tensors were determined by measuring the hyperfine splittings while rotating the direction of a weak ($\sim$300 G) magnetic field. The hyperfine spectra were recorded using Raman-heterodyne spectroscopy, an radio-frequency optical double resonance technique. For both materials magnetic field values were identified where there is no first order Zeeman shift in a europium hyperfine transition. These field insensitive transitions will have application in achieving very long hyperfine coherence times.

I. INTRODUCTION

The coherent optical spectroscopy of rare-earth ion dopants provides a pathway to possible quantum computation and communication devices.[1–5]

Very long optical coherence times[6] are possible in rare-earth ion systems, however historically the hyperfine coherence times have been relatively short. Often the hyperfine coherence times are only slightly longer than the optical coherence times. The dominant hyperfine dephasing mechanism is the magnetic field fluctuations with the nuclear spins in the crystal host. This dephasing mechanism can be greatly reduced by using transitions with zero first order Zeeman shift (ZEFOZ transitions), such transitions can be found at particular field values because of the interplay between the anisotropic pseudoquadrupole and Zeeman terms in the spin Hamiltonian. Using a ZEFOZ transition coherence times approaching one second have been observed[7] in $Pr:Y_2SiO_5$ and using dynamic decoherence control techniques this has been extended to half a minute.[8] When using electromagnetically induced transparency (EIT) to perform light storage, the length of time that the light can be stored is determined by the coherence time for the ground state transition. The ZEFOZ technique enabled light storage for times greater than one second,[9] much longer than has proved possible in atomic systems.

$Pr:Y_2SiO_5$ was used for the initial exploration of the ZEFOZ technique, because its hyperfine structure had been well characterized.[10] Here we present results of the hyperfine characterization of two other rare-earth ion systems, $Eu:Y_2SiO_5$ and $EuCl_3\cdot6H_2O$, and show that the ZEFOZ technique will be applicable for these materials.

Europium-doped yttrium orthosilicate ($Eu:Y_2SiO_5$) is an attractive system for quantum computation, its very long optical coherence times has lead to it being used in a number of quantum computing demonstrations.[4,5] The small nuclear magnetic moment of europium and the very long population lifetimes suggest it is a good candidate for long hyperfine coherence times.

The crystal $EuCl_3\cdot6H_2O$ contains europium not as a dopant but in stoichiometric quantities. In contrast to doped systems where the dopants inevitably cause some distortion of the crystal lattice, $EuCl_3\cdot6H_2O$ can provide a very high density of europium ions in a system with very little crystal strain.[11] The high density and low strain lead to samples that are very optically thick with very low inhomogeneous broadening, which is attractive for quantum optics proposals based on atomic ensembles.[12]

II. HYPERFINE STRUCTURE FOR RARE-EARTH DOPANTS

The theory of hyperfine interactions has been covered elsewhere[10,13] so only a brief treatment will be given here.

The following Hamiltonian describes the europium nucleus and f electrons,

$$H = \{H_{\text{FI}} + H_{\text{CF}}\} + \{H_{\text{HF}} + H_Q + H_z + H_Z\}. \quad (1)$$

The six terms on the right represent the free ion, crystal field, hyperfine, nuclear quadrupole, electronic Zeeman, and nuclear Zeeman Hamiltonians, respectively. The first group of terms are much larger than the second and are what determine the electronic energy levels. In the systems under consideration there is no net electron spin or orbital angular momentum and as such the second group of terms on the right of Eq. (1) are all of similar magnitude and it is the perturbation from these terms that adds hyperfine structure to the electronic levels.

Treating the second group of terms in Eq. (1) as second order perturbations to the first group gives the effective spin Hamiltonian[14]

$$H = \mathbf{B} \cdot (g_J^2\mu_B^2\mathbf{\Lambda}) \cdot \mathbf{B} + \mathbf{B} \cdot (\gamma_N\mathbf{E} + 2A_Jg_J\mu_B\mathbf{\Lambda}) \cdot \mathbf{I} + \mathbf{I}$$
$$\cdot (A_J^2\mathbf{\Lambda} + \mathbf{T}_Q) \cdot \mathbf{I} \quad (2)$$

$$= \mathbf{B} \cdot (g_J^2\mu_B^2\mathbf{\Lambda}) \cdot \mathbf{B} + \mathbf{B} \cdot \mathbf{M} \cdot \mathbf{I} + \mathbf{I} \cdot \mathbf{Q} \cdot \mathbf{I}. \quad (3)$$

The tensor $\mathbf{\Lambda}$ is given by

$$\Lambda_{\alpha\beta} = \sum_{n=1}^{2J+1} \frac{\langle 0|J_\alpha|n\rangle\langle n|J_\beta|0\rangle}{\Delta E_{n,0}}; \quad (4)$$

also $\mathbf{E}$ is the 3×3 identity matrix, $\mathbf{B}$ is the magnetic field, and $\mathbf{I}$ is the vector of nuclear spin operators, g_J is the Landé

$\pm 1/2$ ⎯⎯⎯

$\pm 1/2$ ⎯⎯⎯

34.5 MHz   27.0 MHz

$\pm 3/2$ ⎯⎯⎯ $\pm 3/2$ ⎯⎯⎯

46.2 MHz   29.0 MHz

$\pm 5/2$ ⎯⎯⎯

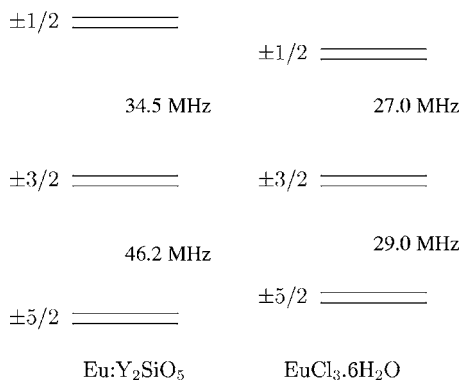$\pm 5/2$ ⎯⎯⎯

Eu:Y_2SiO_5 $EuCl_3 \cdot 6H_2O$

FIG. 1. The hyperfine level structure in zero magnetic field for [151]Eu, for the ground electronic state of the two systems investigated in this work. These splittings were first measured by Yano *et al.* for Eu:Y_2SiO_5 (Ref. [16]) and Martin *et al.* for $EuCl_3 \cdot 6H_2O$ (Ref. [11]).

g value, γ_N is the nuclear gyromagnetic ratio, and A_J is the hyperfine interaction parameter. The term $\mathbf{I} \cdot \mathbf{T}_Q \cdot \mathbf{I}$ describes the nuclear electric quadrupole interaction. The term $A_J^2 \mathbf{I} \cdot \mathbf{\Lambda} \cdot \mathbf{I}$, which has the same form, is due to the second order magnetic hyperfine, also known as the pseudoquadrupole interaction.[15]

For this work the first term in Eq. (2) was neglected, as it makes no changes to the hyperfine splittings and has only a small effect on the optical frequency for the small magnetic field values used. The Hamiltonian used to fit the data can be written as

$$H = \mathbf{B} \cdot \mathbf{M} \cdot \mathbf{I} + \mathbf{I} \cdot \mathbf{Q} \cdot \mathbf{I}. \tag{5}$$

Hence the goal of this work was to determing the effective Zeeman $\mathbf{M}$ and quadrupole $\mathbf{Q}$ tensors for the systems studied.

Both the stable isotopes of europium have a nuclear spin of 5/2. In zero magnetic field the quadrupolar term splits the hyperfine states into three pairs of degenerate levels. The zero field magnetic field energy level diagrams for the ground state hyperfine structures, for the two systems studied in this work are shown in Fig. 1.

III. THE MATERIAL SYSTEMS

There are two stable europium isotopes [151]Eu and [153]Eu which occur in approximately equal concentrations. This work concentrated on the 151 isotope. When compared to [153]Eu, the [151]Eu isotope has a larger nuclear magnetic moment and a smaller electric quadrupole moment. This combination suggests that magnetic fields required to use the ZEFOZ technique will be smaller for [151]Eu. Against this choice is the expected smaller second order Zeeman shifts for ZEFOZ transitions for [153]Eu, again because of smaller magnetic dipole moment and larger quadrupole splittings for [153]Eu. So by using [153]Eu it is expected one would obtain (even) longer coherence times but with the requirement of higher magnetic fields.

The Y_2SiO_5 structure has symmetry given by the C_{2h}^6 space group with four formula units of Y_2SiO_5 per transla-

tional unit. This gives eight different positions at which europium can replace yttrium. The four positions, each with C_1 (no) point symmetry, can be divided into two sets with the members of each set related to each other by the crystals C_2 axis and inversions. The measurements presented here are of one set, "site 1"[17] which exhibits the longer optical coherence times.

The doping of europium in the Y_2SiO_5 sample used was 0.1%.

The $EuCl_3 \cdot 6H_2O$ structure has symmetry given by the C_{2h}^4 subgroup with the europium ions sitting in a site with point symmetry C_2 and exist in two different, but magnetically equivalent, orientations related by an inversion.

IV. EXPERIMENT

The crystal was cooled to liquid helium temperatures and mounted in a set of small superconducting *XYZ* coils which enabled fields of ~300 G to be generated with currents ~3 A.

To take Raman-heterodyne,[18,19] spectra light from a frequency stabilized dye laser (1 MHz) was incident on the sample. The frequency of the light was tuned to be resonant with the transition from $^7F_0$ to $^5D_0$. A swept radio-frequency (RF) field was applied to the sample using a six turn coil wrapped around the sample. When the RF field is resonant with a hyperfine transition a coherence is produced between the hyperfine levels. This coherence, along with that induced by the laser creates another optical field with the same mode characteristics as the laser and a frequency shift given by the RF frequency. This frequency shifted optical field is detected as beat on the transmitted light. The task of generating the RF driving signal and analyzing the detected signal was carried out using a network analyzer. The output from the network analyzer was averaged on a digital oscilloscope and then stored on a PC. Along with computer controlled current supplies, this enabled autonomous collection of the data.

The laser power used was approximately one milliwatt and it was focused from a 1 mm collimated beam with a 20 cm lens. One watt of RF power was used and the network analyzer swept at a rate of a few hertz.

In the case of Eu:Y_2SiO_5 an optical repumping beam was needed to observe a Raman heterodyne signal. The transitions driven are shown in Fig. 2. It is noteworthy that neither scanning the laser nor redistributing hyperfine populations with an RF driving resulted in a signal. We believe this is because the optical pumping beam is important for more than just overcoming spectral holeburning. Theoretically it can be shown that you should not expect a Raman heterodyne signal in a system where the optical inhomogeneous broadening is large compared to the hyperfine splittings.[20] This is because in a situation where each of the excited states contributes equally to the Raman heterodyne signal, their contributions will sum to zero. The optical pumping overcomes this problem by redistributing population to break this symmetry. However it should also be appreciated that the arguments of Alexander[20] suggest that one should not observe a Raman heterodyne signal in many other rare-earth ion systems where they are observed experimentally. We believe that this
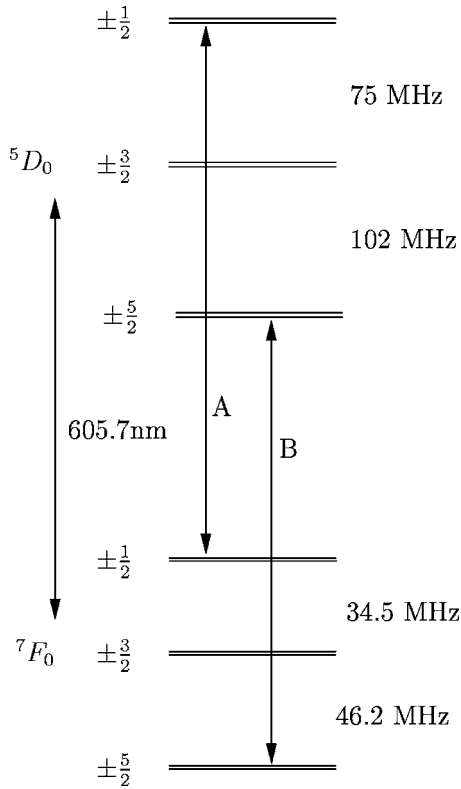
FIG. 2. Optical repumping scheme for $Eu:Y_2SiO_5$. When measuring the $\pm 1/2 \leftrightarrow \pm 3/2$ transitions field. A takes on the role of probe beam and field B repump. When investigating the $\pm 3/2 \leftrightarrow \pm 5/2$ transitions the roles are reversed.

is due to relaxation mechanisms (which are too small to be effective in $Eu:Y_2SiO_5$) breaking the symmetry.

V. RESULTS

On applying a small magnetic field to $Eu:Y_2SiO_5$ each one of the $\pm a/2 \leftrightarrow \pm b/2$ manifolds splits into eight lines. Removing the degeneracy of the $\pm x/2$ states results in four possible transitions, two sets of these four are observed because of the two different orientations of the ions' environment. For $EuCl_3 \cdot 6H_2O$ the two orientations are magnetically equivalent and so a four line pattern is observed.

For the $\pm 1/2 \leftrightarrow \pm 3/2$ and $\pm 3/2 \leftrightarrow \pm 5/2$ manifolds of both $EuCl_3 \cdot 6H_2O$ and $Eu:Y_2SiO_5$ spectra were taken for 200 different magnetic field values. The two hundred stacked spectra for the $\pm 1/2 \leftrightarrow \pm 3/2$ manifold in $Eu:Y_2SiO_5$ are shown in Fig. 3. The magnetic field values are shown in Fig. 4, they trace out a spiral wrapped around an ellipsoid.

VI. EXTRACTING SPIN HAMILTONIAN PARAMETERS

The positions of all the peaks were determined manually from the recorded spectra and the simulated annealing method described in Ref. 10 was used to extract the parameters of the spin Hamiltonian.

Along with the orientation of the principal axes two parameters are required to determine the pseudoquadrupole
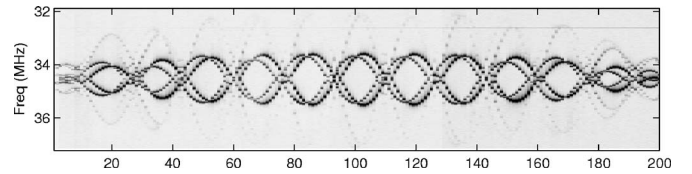

FIG. 3. Image showing the experimentally obtained spectra for the $\pm 1/2 \leftrightarrow \pm 3/2$ transition in EuY_2SiO_5. Each vertical slice is a spectra for a particular magnetic field value with the darkness denoting the strength of the Raman heterodyne signal.

tensors. For $Eu:Y_2SiO_5$ the following parametrization was used:

$$\mathbf{Q}_1 = R(\alpha_Q,\beta_Q,\gamma_Q) \begin{bmatrix} -E & 0 & 0 \\ 0 & E & 0 \\ 0 & 0 & D \end{bmatrix} R^T(\alpha_Q,\beta_Q,\gamma_Q), \quad (6)$$

where $R(\alpha,\beta,\gamma)$ is the rotation matrix defined by the three Euler angles (α,β,γ),

$$R(\alpha,\beta,\gamma) = \begin{bmatrix} \cos\alpha & -\sin\alpha & 0 \\ \sin\alpha & \cos\alpha & 0 \\ 0 & 0 & 1 \end{bmatrix} \times \begin{bmatrix} \cos\beta & 0 & \sin\beta \\ 0 & 1 & 0 \\ -\sin\beta & 0 & \cos\beta \end{bmatrix}$$

$$\times \begin{bmatrix} \cos\gamma & -\sin\gamma & 0 \\ \sin\gamma & \cos\gamma & 0 \\ 0 & 0 & 1 \end{bmatrix}. \quad (7)$$

For the Zeeman tensor there are six independent parameters in general and the following parametrization was used:

$$\mathbf{M}_1 = R(\alpha_M,\beta_M,\gamma_M) \begin{bmatrix} g_x & 0 & 0 \\ 0 & g_y & 0 \\ 0 & 0 & g_z \end{bmatrix} R^T(\alpha_M,\beta_M,\gamma_M). \quad (8)$$

The parameters describing the quadrupole and Zeeman tensors and the position of the C_2 axis were determined by minimizing the difference between the experimental field
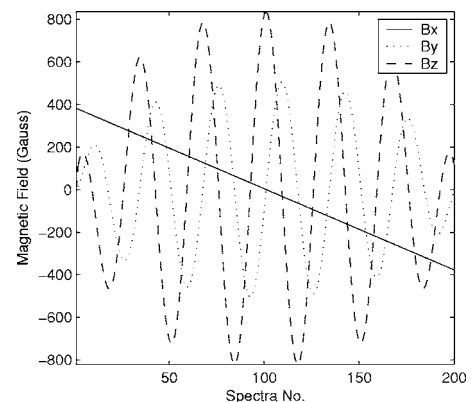

FIG. 4. The 200 magnetic field values that were used to gather each of the hyperfine spectra rotation patterns.

values and what could be expected from a pair of systems with Hamiltonians

$$H_1 = \mathbf{B} \cdot \mathbf{M}_1 \cdot \mathbf{I} + \mathbf{I} \cdot \mathbf{Q}_1 \cdot \mathbf{I},$$

$$H_2 = \mathbf{B} \cdot \mathbf{M}_2 \cdot \mathbf{I} + \mathbf{I} \cdot \mathbf{Q}_2 \cdot \mathbf{I}. \quad (9)$$

Here each $\mathbf{X}_1$ and $\mathbf{X}_2$ are related to each other via the C_2 axis, the position of which was specified by the two parameters

$$\mathbf{R}_{C_2} = (\cos\phi\sin\theta, \ \sin\phi\sin\theta, \cos\theta). \quad (10)$$

So θ specifies the angle the C_2 axis makes with the the z axis and ϕ is the angle that the projection of the C_2 axis on to the xy plane makes with the x axis.

For EuCl$_3\cdot$6H$_2$O the C_2 symmetry of the site dictates that for both $\mathbf{M}$ and $\mathbf{Q}$ one of the principal axes must lie along the C_2 axis and the other two in a plane perpendicular to it. Because of this the $\mathbf{M}$ and $\mathbf{Q}$ tensors were parametrized,

$$\mathbf{Q} = R(\alpha,\beta,\gamma_Q)\begin{bmatrix} -E & 0 & 0 \\ 0 & D & 0 \\ 0 & 0 & E \end{bmatrix} R^T(\alpha,\beta,\gamma_Q),$$

$$\mathbf{M} = R(\alpha,\beta,\gamma_M)\begin{bmatrix} g_x & 0 & 0 \\ 0 & g_y & 0 \\ 0 & 0 & g_z \end{bmatrix} R^T(\alpha,\beta,\gamma_M). \quad (11)$$

Choosing Euler angles α and β the same for both rotations means that the principal axes that were both in the z direction for the diagonal tensors will still be both in the same direction. This way the α and β define the direction of the C_2 axis. In the parametrization of the $\mathbf{Q}$ tensor the order of the eigenvalues has been changed, this is because the eigenvalue corresponding to the direction of the C_2 axis is E.

The results here are given in terms of the lab coordinate system defined by the XYZ coils. For both materials the position of the C_2 axis was nominally along the z axis but was allowed to vary as a parameter because of the misalignment between the coils and the sample this was of the order of 10°. Other than the position of the C_2 axis, which could be determined from the results taken, the relationship between the lab coordinate system and the crystallographic axes of the crystal was not known. Orientating Eu:Y$_2$SiO$_5$ to match our orientation will be helped by the observation that when a beam is directed along the C_2 axis the optical transition is partly polarized. The maximum absorption occurs when the light is polarized along our x direction, with an uncertainty of about 10°.

The parameters D and E were allowed to vary from the values determined by the zero field splittings because the zero field lines were broader than those observed for the magnetic field. This was a result of a small background magnetic field.

The results of the fitting are shown in Fig. 5 and Fig. 6 and the parameters inferred are tabulated in Table I and Table II. The rms difference between calculated and observed peak positions was 15 kHz for Eu:Y$_2$SiO$_5$ and 7.4 kHz for EuCl$_3\cdot$6H$_2$O, in both cases much smaller than the observed
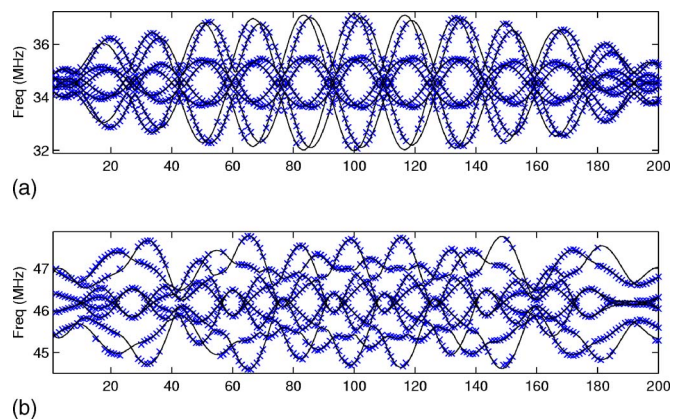

(a)

(b)

FIG. 5. (Color online) The peak positions from the measured spectra for Eu:Y$_2$SiO$_5$ are shown with the crosses for each of the 200 spectra taken. The lines are the transition frequencies calculated from the extracted spin Hamiltonian parameters.

linewidths. Also tabulated are the uncertainties calculated assuming all errors are Gaussian random noise in the peak frequencies. In reality the effect of such errors are much smaller than the systematic errors. The major systematic errors influencing the result are errors in the calibration of the field coils of approximately 5% and errors in determining the peaks positions of what are in some cases asymmetric spectral lines. As our results are reported in terms of our laboratory XYZ frame, there is no uncertainty due to misalignment of the sample. For results that were given in terms of the crystal axes and where the 5% uncertainty in the calibration of the coils was taken into account, the results of Tables I and II can be used but with uncertainties of 5% in the g values and 10° in the angles.

VII. TRANSITIONS WHERE THERE IS ZERO FIRST ORDER ZEEMAN SHIFT

Given the spin Hamiltonians determined in the above section one can find magnetic field values were there is no first
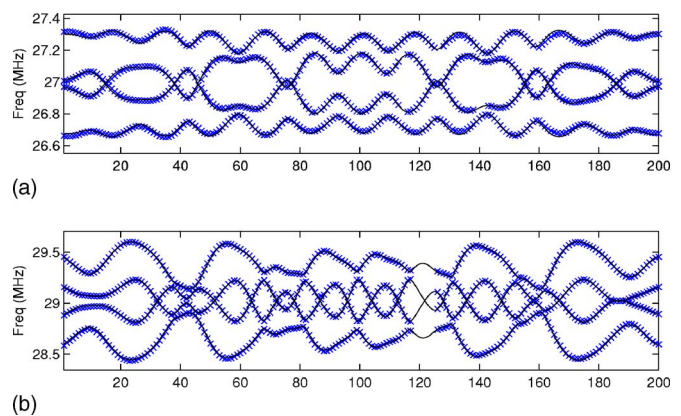

(a)

(b)

FIG. 6. (Color online) The peak positions from the measured spectra for EuCl$_3\cdot$6H$_2$O are shown with the crosses for each of the 200 spectra taken. The lines are the transition frequencies calculated from the extracted spin Hamiltonian parameters.

TABLE I. Spin Hamiltonian parameters for Eu:YSO with coordinates defined by the *XYZ* coil axes. The Δ values are the uncertainty in the fit, systematic errors such as the uncertainty in the calibration of the magnetic field coils is not included.

Quantity	Value	Δ	Units
α_M	144.9	0.1	degrees
β_M	34.9	0.1	degrees
γ_M	98.1	0.6	degrees
g_1	0.443	0.002	kHz/G
g_2	0.5682	0.0007	kHz/G
g_3	1.1183	0.0010	kHz/G
$C_2\theta$	10.11	0.03	degrees
$C_2\phi$	165.2	0.2	degrees
α_Q	−39.3	0.2	degrees
β_Q	76.49	0.06	degrees
γ_Q	149.9	0.1	degrees
E	2.73500	0.00007	MHz
D	12.3797	0.0001	MHz

order change in the a transition frequency with magnetic field. Such a situation is shown in Fig. 7

To find ZEFOZ transitions we used first and second order time independent perturbation theory to calculate first order and second order Zeeman coefficients for a given energy level.

$$\frac{\partial}{\partial B_i}\omega_k(\mathbf{B}) = \langle \phi_k(\mathbf{B})|M_{ij}I_j|\phi_k(\mathbf{B})\rangle, \qquad (12)$$

$$\frac{\partial^2}{\partial B_i \partial B_j}\omega_k(\mathbf{B}) = \sum_{l \neq k} \frac{\langle \phi_k(\mathbf{B})|M_{in}I_n|\phi_l(\mathbf{B})\rangle\langle \phi_l(\mathbf{B})|M_{jm}I_m|\phi_k(\mathbf{B})\rangle}{\omega_k(\mathbf{B}) - \omega_l(\mathbf{B})}. \qquad (13)$$

Subtracting these expressions to obtain results for transition frequencies, one can easily find the Zeeman gradient vector and curvature tensor,

TABLE II. Results for EuCl$_3$·6H$_2$O with coordinates defined by the *XYZ* coil axes. The Δ values are the uncertainty in the fit, systematic errors such as the uncertainty in the calibration of the magnetic field coils is not included.

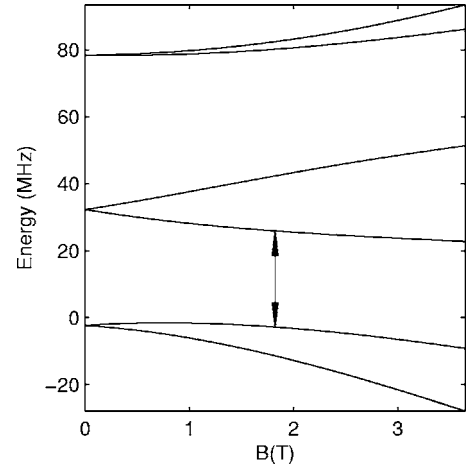| Quantity	Value	Δ	Units
α_M	−80	2	degrees
β_M	9.7	0.4	degrees
γ_M	143	2	degrees
g_1	150.13	0.08	Hz/G
g_2	390.3	0.2	Hz/G
g_3	280.4	0.3	Hz/G
γ_Q	123	2	degrees
E	2.4663	0.0002	MHz
D	8.1128	0.0003	MHz

FIG. 7. An example of a ZEFOZ transition. The graph shows the calculated energy levels for one orientation of Eu:Y$_2$SiO$_5$ as a magnetic field is increased from zero in a particular direction. At 1.82 T, for the transition marked, the slope of the two energy levels with magnetic field are equal. This means that, to first order, a change in the radial magnetic field component will have no effect on the transition frequency and cause no dephasing. Not shown in this figure is that the the transition frequency is also insensitive to field changes in the other two dimensions.

$$v_i^{kl}(\mathbf{B}) = \frac{\partial}{\partial B_i}\omega_{kl}(\mathbf{B}),$$

$$C_{ij}^{kl}(\mathbf{B}) = \frac{\partial^2}{\partial B_i \partial B_j}\omega_{kl}(\mathbf{B}). \qquad (14)$$

Here $\omega_{kl} = \omega_k - \omega_l$ is the frequency difference between the kth and the lth energy level.

The ZEFOZ transitions we are looking for is where $\mathbf{v}^{kl}(\mathbf{B}) = 0$. This can be found rapidly by the iteration

$$\mathbf{B}_{\text{new}} \leftarrow \mathbf{B} - 2\mathbf{C}^{-1}\mathbf{v} \qquad (15)$$

if $\mathbf{B}$ is close enough to the ZEFOZ transitions for the frequency region encompassing both to be approximated by a quadratic function.

Such ZEFOZ transitions were tabulated by starting the search on a three dimensional grid of magnetic field values. The weakness of the search method was the grid has to be made fine in order to find ZEFOZ transitions with high curvature. We probably have not found all the ZEFOZ transitions but we are confident that we have found all the lowest curvature ZEFOZ transitions. Fortunately it is precisely these low curvature ZEFOZ transitions that are of interest for generating long coherence times. After making the grids twice as coarse, the procedure failed to find only a handful of the ZEFOZ transitions. The ZEFOZ transitions that were missed with the coarser grids had curvatures among the highest.

Beyond a certain magnetic field value the energy levels will vary linearly with magnetic field as the Zeeman term dominates the pseudoquadrupole term, for this reason we can be confident that there are no ZEFOZ transitions at magnetic fields larger than where we searched. The mesh size for the search for ZEFOZ transitions used was 60 G for Pr:Y$_2$SiO$_5$,
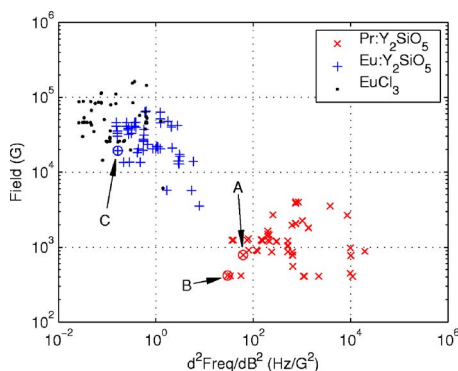
FIG. 8. (Color online) A scatter plot showing the different ZE-FOZ transitions that have been identified for three systems. The magnetic field required is plotted vs the second order Zeeman dependence. The second order Zeeman coefficient is a tensor valued quantity, it is reduced to a single number by taking the largest of the absolute values of the eigenvalues. According to the spin Hamiltonians determined here and in Ref. 10 the ZEFOZ transitions marked A, B, and C occur at magnetic fields of (−732 G, −173 G, 219 G), (−104 G, −378 G, −143 G) and (1.77 T, −0.63 T, −0.45 T) and have transition frequencies of 8.65 MHz, 7.27 MHz, and 29.18 MHz.

1 kG for $Eu:Y_2SiO_5$, and 2 kG for $EuCl_3 \cdot 6H_2O$.

All the ZEFOZ transitions found for the two systems measured in this work are shown in Fig. 8. Also shown are the ZEFOZ transitions found for $Pr:Y_2SiO_5$, the only system to date where the ZEFOZ technique has been applied. For each of the three systems approximately 60 ZEFOZ points were found.

It should be noted that the magnetic field values required for the ZEFOZ technique to be applied in $Eu:Y_2SiO_5$ and $EuCl_3 \cdot 6H_2O$ are much higher than the fields used for the characterization employed here. This "extrapolation" to higher field values is possible because the low field measurements determine the spin-Hamiltonian parameters and the spin-Hamiltonian is valid up to very large fields. This ability to gather the required information using low magnetic field data and then use the characterization at higher fields was demonstrated in the ZEFOZ work on $Pr:Y_2SiO_5$.[7,8,10]

As has been reported in previous work,[8] being very close to the ZEFOZ field value is required for the long coherence times to be observed. An accuracy better than one part in one thousand was required in Ref. 8. The ZEFOZ field values calculated in this work will be limited by the 5% uncertainty in the calibration of the field coils which may not be precise enough to obtain the longest coherence times. The procedure used in Refs. 7 and 8 was to start at the calculated field and then tweak from this field to the ZEFOZ field in a two step process. The first step was to adjust the magnetic field and observe the transition frequency and the second was to adjust the field to maximize the coherence time measured with spin echoes.

VIII. PROJECTED COHERENCE TIMES

The two circled points for $Pr:Y_2SiO_5$ are those for which coherence times have been measured. The one labeled "A"

was where the long coherence times[7,8] using this technique were first demonstrated and where the long term stopped light experiments were carried out.[9] The one labeled "B" was identified in this work and is on the face of it superior. The curvature is flatter, suggesting longer coherence times and the magnetic fields required are smaller (∼420 G). In recent spin echo experiments we have measured a slightly longer coherence time of 1.4 s (compared to 0.8 s for "A"). The dynamic decoupling techniques which have proved so effective in extending the coherence time for "A"[8] have not yet been investigated for "B."

The ZEFOZ transitions of the europium systems have much smaller second order Zeeman dependence than for $Pr:Y_2SiO_5$, suggesting longer coherence times can be achieved. This assertion can be to some extent quantitative because magnetic field fluctuations causing dephasing should have the same origin in both $Pr:Y_2SiO_5$ and $Eu:Y_2SiO_5$, namely the yttrium nuclear spins.

Using a very simple model of dephasing one arrives at

$$\frac{1}{t_2} = S_2(\Delta B)^2, \tag{16}$$

where S_2 is the second order Zeeman coefficient, defined here as the largest of the absolute values of the eigenvalues of $\mathbf{C}$, t_2 is the coherence time, and $(\Delta B)^2$ is the variance of the magnetic field fluctuations. This model can be thought of as the result of a simple second order power series expansion of the transition frequency as a function of magnetic field

$$\Delta f = S_2(\Delta B)^2. \tag{17}$$

The ZEFOZ transition "A," occuring at around 780 G for $Pr:Y_2SiO_5$, has a t_2 of 0.8 s and a second order Zeeman coefficient of 60 Hz/G^2. From this one infers a fluctuating magnetic field of $\sqrt{(\Delta B)^2}$=0.14 G. This is consistent with the field one would expect from a yttrium nucleus at the dopant-yttrium separations in Y_2SiO_5.[21] To give an example of the coherence times that may be possible in $Eu:Y_2SiO_5$, the ZEFOZ transition marked "C" in Fig. 8, occurs at a field of 1.9 T±5% and has a second order Zeeman coefficient of 0.17 Hz/G^2. This second order Zeeman coefficient is 370 times smaller than for the "A" transition in $Pr:Y_2SiO_5$, suggesting possible coherence times of the order of hundreds of seconds (370 times longer than the 0.8 s that has been measured for $Pr:Y_2SiO_5$ at "A"). The dynamical decoupling techniques that have been very successful in extending the coherence time for $Pr:Y_2SiO_5$ at ZEFOZ transitions from 0.8 s to tens of seconds, should be just as applicable for the $Eu:Y_2SiO_5$ system, suggesting that even longer coherence times will be possible. An exciting possibility from a fundamental point of view is that a situation where the effect of magnetic dephasing so greatly reduced will be a good test of our current understanding of dephasing mechanisms.[21]

The $EuCl_3 \cdot 6H_2O$ system displays even flatter ZEFOZ transitions, however, this will be to some extent offset by the larger magnetic fluctuations in the hydrated crystal due to the large nuclear magnetic moment of the protons in the water.

IX. CONCLUSION

By taking spectra while rotating the orientation of a small magnetic field we have determined the parameters of the spin Hamiltonians describing the hyperfine structure of ^{151}Eu in Eu:Y_2SiO_5 and $EuCl_3 \cdot 6H_2O$. The spin Hamiltonian allows one to determine all the transition frequencies and oscillator strengths for hyperfine transitions for different magnetic fields. We used the derived spin Hamiltonians to find magnetic field values where a transition frequency is insensitive to magnetic field perturbations. As the dominant dephasing mechanism is magnetic field fluctuations from nuclear spins in the host, long hyperfine coherence times should be expected in such situations. A simple comparison with Pr:Y_2SiO_5, where such coherence times have been measured, suggests hyperfine coherence times of hundreds of seconds will be possible with Eu:Y_2SiO_5 at field values of about 1.9 T. The dynamic decoherence techniques,[8] which were very successful in extending the coherence times of Pr:Y_2SiO_5, should be just as applicable for Eu:Y_2SiO_5, leading to even longer coherence times.

---

*Electronic address: jevon.longdell@anu.edu.au

[1] N. Ohlsson, R. K. Mohan, and S. Kröll, Opt. Commun. **201**, 71 (2002).

[2] M. Nilsson, L. Rippe, N. Ohlsson, T. Christiansson, and S. Kröll, Phys. Scr., T **T102**, 178 (2002).

[3] K. Ichimura, Opt. Commun. **196**, 119 (2001).

[4] J. J. Longdell and M. J. Sellars, Phys. Rev. A **69**, 032307 (2004).

[5] J. J. Longdell, M. J. Sellars, and N. B. Manson, Phys. Rev. Lett. **93**, 130503 (2004).

[6] R. W. Equall, Y. Sun, R. L. Cone, and R. M. Macfarlane, Phys. Rev. Lett. **72**, 2179 (1997).

[7] E. Fraval, M. J. Sellars, and J. J. Longdell, Phys. Rev. Lett. **92**, 077601 (2004).

[8] E. Fraval, M. J. Sellars, and J. J. Longdell, Phys. Rev. Lett. **95**, 030506 (2005).

[9] J. J. Longdell, E. Fraval, M. J. Sellars, and N. B. Manson, Phys. Rev. Lett. **95**, 063601 (2005).

[10] J. J. Longdell, M. J. Sellars, and N. B. Manson, Phys. Rev. B **66**, 035101 (2002).

[11] J. P. D. Martin, M. J. Sellars, P. Tuthill, N. B. Manson, G. Pryde, and T. Dyke, J. Lumin. **78**, 19 (1998).

[12] L. M. Duan, M. D. Lukin, J. I. Cirac, and P. Zoller, Nature (London) **414**, 413 (2001).

[13] *Spectroscopy of Solids Containing Rare Earth Ions*, edited by A. A. Kaplyanskii and R. M. Macfarlane (North-Holland, Amsterdam, 1987), Chap. 1, p. 51.

[14] M. A. Teplov, Sov. Phys. JETP **26**, 872 (1968).

[15] J. M. Baker and B. Bleaney, Proc. R. Soc. London, Ser. A **245**, 156 (1958).

[16] R. Yano, M. Mitsunaga, and N. Uesugi, J. Opt. Soc. Am. B **9**, 992 (1992).

[17] R. Yano, M. Mitsuanga, and N. Uesugi, Opt. Lett. **16**, 1884 (1991).

[18] J. Mlynek, N. C. Wong, R. G. DeVoe, E. S. Kintzer, and R. G. Brewer, Phys. Rev. Lett. **50**, 993 (1983).

[19] N. C. Wong, E. S. Kintzer, J. Mlynek, R. G. DeVoe, and R. G. Brewer, Phys. Rev. B **28**, 4993 (1983).

[20] A. L. Alexander (unpublished).

[21] E. Fraval, Ph.D. thesis, Australian National University, 2006.